FRAP – Fluorescence recovery after photobleaching

mobility-diffusion

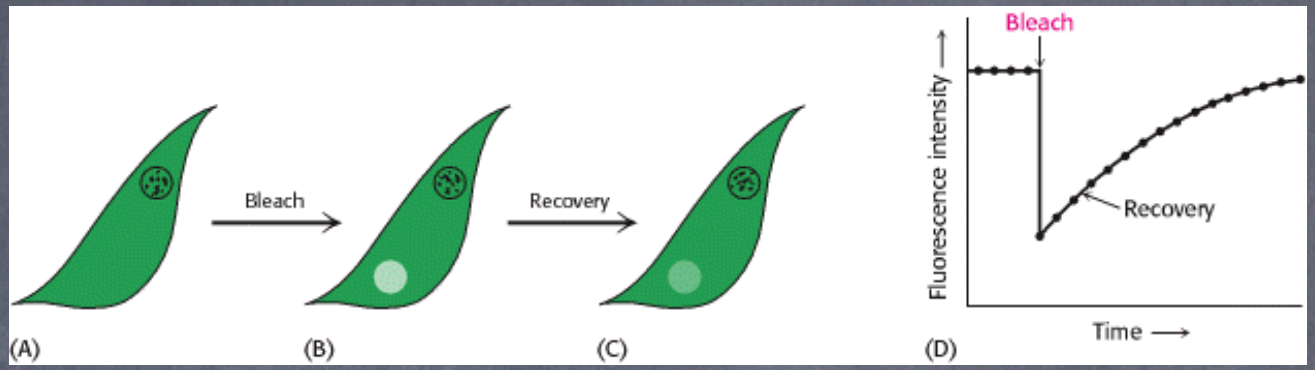

$$D = \frac{w^2}{4t_{\frac{1}{2}}}$$

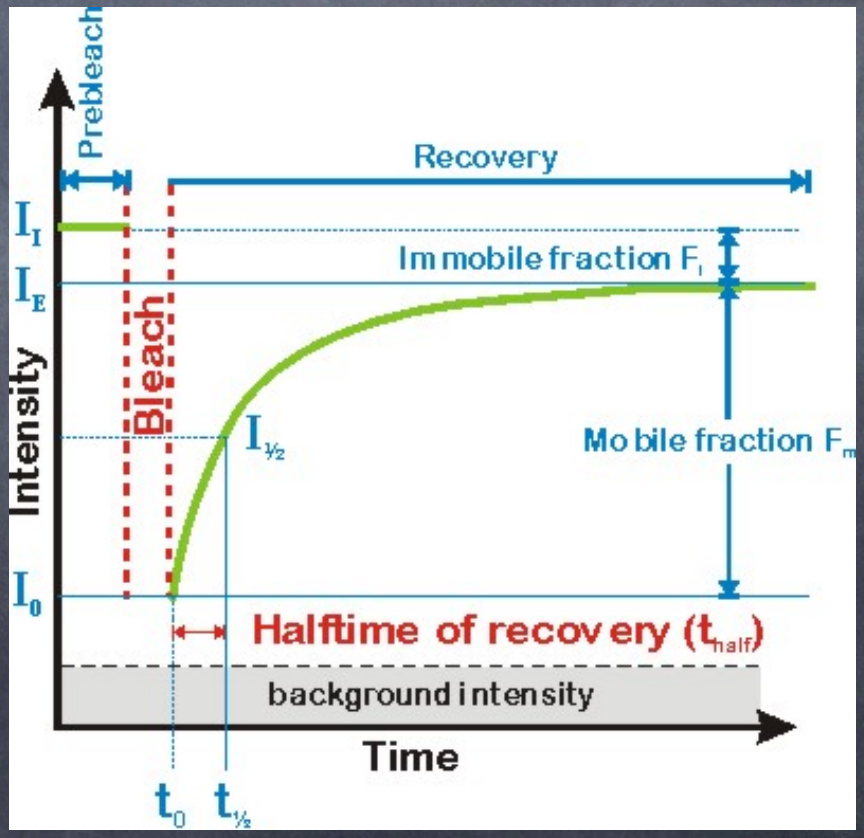

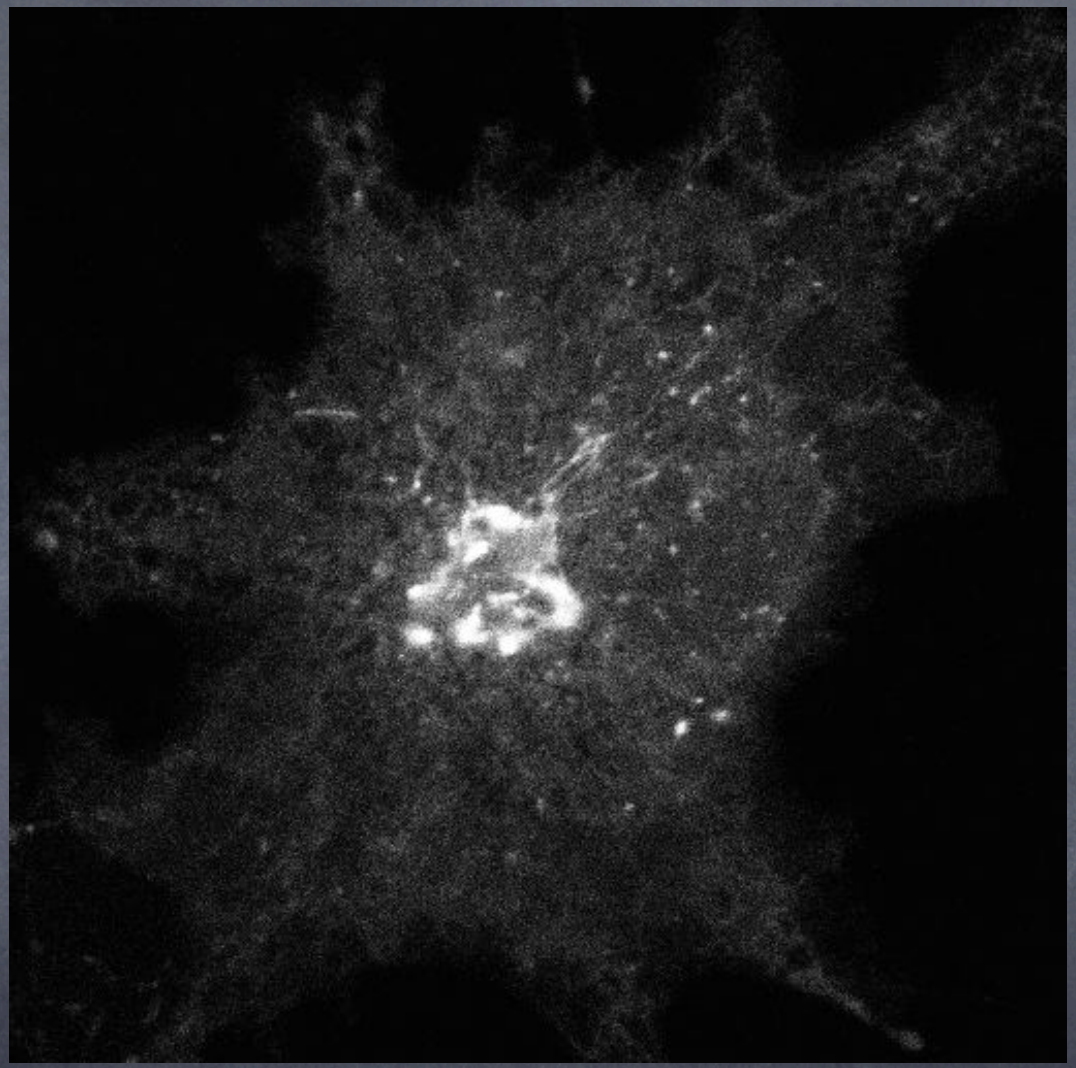

Nucleocytoplasmic shuttling revealed by FRAP and FLIP technologies

Mario Köster, Thomas Frahm and Hansjörg Hauser

Protein mobility within cells is of key importance for many cellular functions. Although immunostaining can reveal protein locations in the steady-state, this might not represent the full picture and provides no information about protein movements. Fluorescence recovery after photobleaching (FRAP) and fluorescence loss in photobleaching (FLIP) are two techniques that enable the dynamics of intracellular protein mobility to be studied. These technologies have been successfully used to analyze the nucleocytoplasmic shuttling of STAT1, an intracellular signal transducer and activator of transcription, and can applied to the study of other proteins. Furthermore, FRAP and FLIP approaches have the added advantage of not affecting cell viability and might find application in the imaging of intracellular events in certain tissues and live animals.

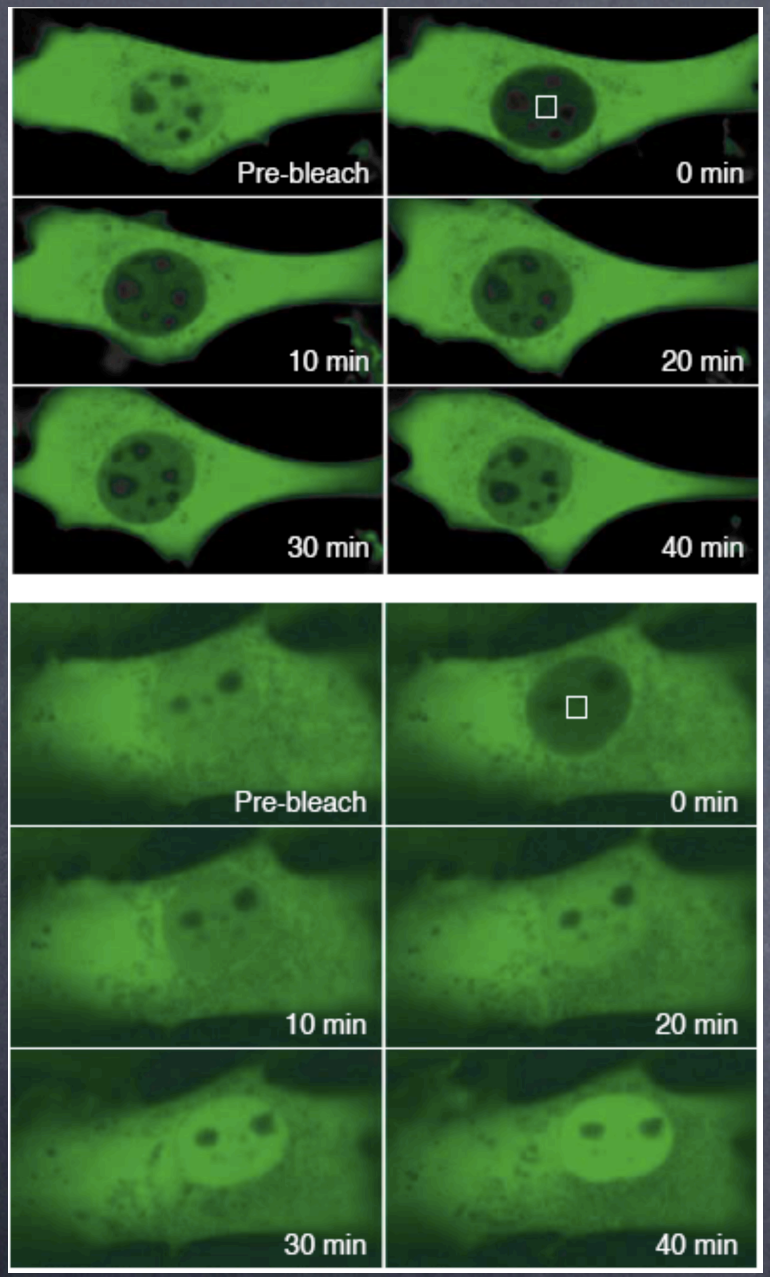
Pre-bleach
0 min
10 min
20 min
30 min
40 min
Pre-bleach
0 min
10 min
20 min
30 min
40 min

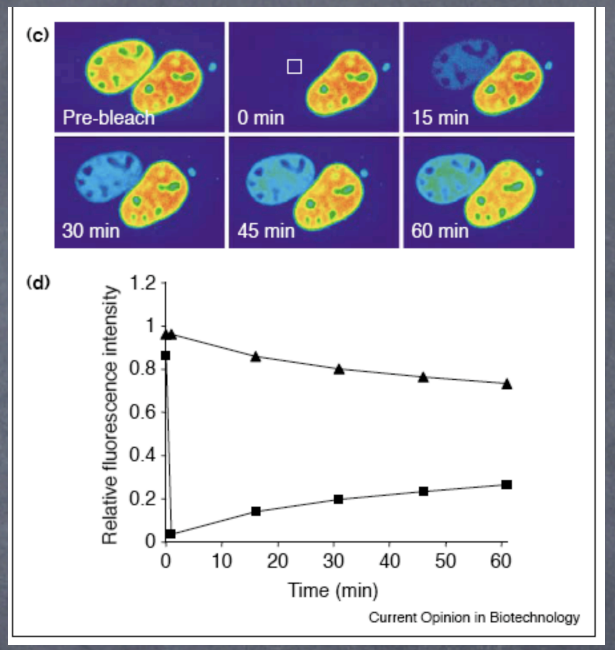
(c)
Pre-bleach
0 min
15 min
30 min
45 min
60 min
(d)
Relative fluorescence intensity
1.2
1
0.8
0.6
0.4
0.2
0
0
10
20
30
40
50
60
Time (min)
Current Opinion in Biotechnology

Nuclear protein mobility determined by FRAP

Type	GFP fusion	Measured mobility	Comments	Ref.
Nucleoplasmic	eGFP	57 μ^2/s in the nucleoplasm		[14]
	Topoisomerase II α and β	$t_{1/2}$ for 1-μm circle 6–10 s in the nucleolus, 2–3 s in the nucleoplasm	Proteins immobilized by inhibitors of topoisomerase activity	[23]
	Topoisomerase I	$t_{1/2}$ for 1-μm circle 1.1 s (nucleoplasm), 1.9 s (nucleolus); 14.3 s (nucleoplasm) and 12.5 s (nucleolus)	Two mobile fractions with distinct kinetics, enzyme relocalized and of reduced mobility when topoisomerase activity is inhibited	[24]
	ZAP-70	>1 μ^2/s (nucleoplasm)		[25]
	Protein phosphatase 1	$t_{1/2} < 30$ s (nucleolus)		[26]
	LMP2 proteosome subunit	Rapid mobility seconds time scale	Movement not inhibited by ATP depletion	[27]
Nucleoplasmic/DNA repair	XRCC1, XPA, XPB	6–15 μ^2/s in absence of UV damage	Proteins immobilized on introduction of DNA damage	[14]
	Ku70, Ku86	0.35 μ^2/s	Reduction in mobility determined by amino acids 255–550	[28]
	Rad proteins	~7.5–15 μ^2/s	Protein mobilities reduced to different extents on introduction of double-strand breaks	[29]
Nuclear body associated	ASF/SF2	0.24 μ^2/s	Mobility increased slightly on inhibition of RNA polymerase II transcription	[17] see also [30]
	Nucleolar proteins	0.019–0.16 μ^2/s in nucleolus 0.51–1.6 μ^2/s in nucleoplasm	Transcription-dependent changes in mobility observed	[31] see also [17,32]
	PML, Sp100	Mostly "immobile" over 15-min time scale	Associated with PML bodies; CBP was shown to be a dynamic component of the PML bodies under the same conditions	[33]
Chromatin associated	Histone H1	220–250 s residency time in mouse, similar in human	Both protein acetylation and protein phosphorylation alter residency times	[34,35]
	Nucleosomal histones	$t_{1/2}$ of 2 or more hours $t_{1/2} \geqslant 2$ h	H2B exchanged more rapidly than H3/H4; part of the exchanging H2B population was dependent on RNA polymerase II transcription	[36]
	HMG17	0.45 μ^2/s		[17]
Transcription factor	Stat1	Approx same as GFP		[37]
	Estrogen receptor	0.8 s—unstimulated, 6 s—stimulated	Estrogen receptor was immobilized by antagonist, ATP depletion, and inhibition of proteosome activity	[38] see also [39]
	Glucocorticoid receptor	"Rapid" seconds time scale	Stimulated receptor has short residency time on its target DNA in living cell system	[40]
	SRC-1	~10 s in presence of estradiol	Mobility reduced in ER cotransfected cells in the presence of estradiol but not other treatments, e.g., inhibitor, that reduce ER mobility	[38]

fluorescence loss in photobleaching (FLIP)

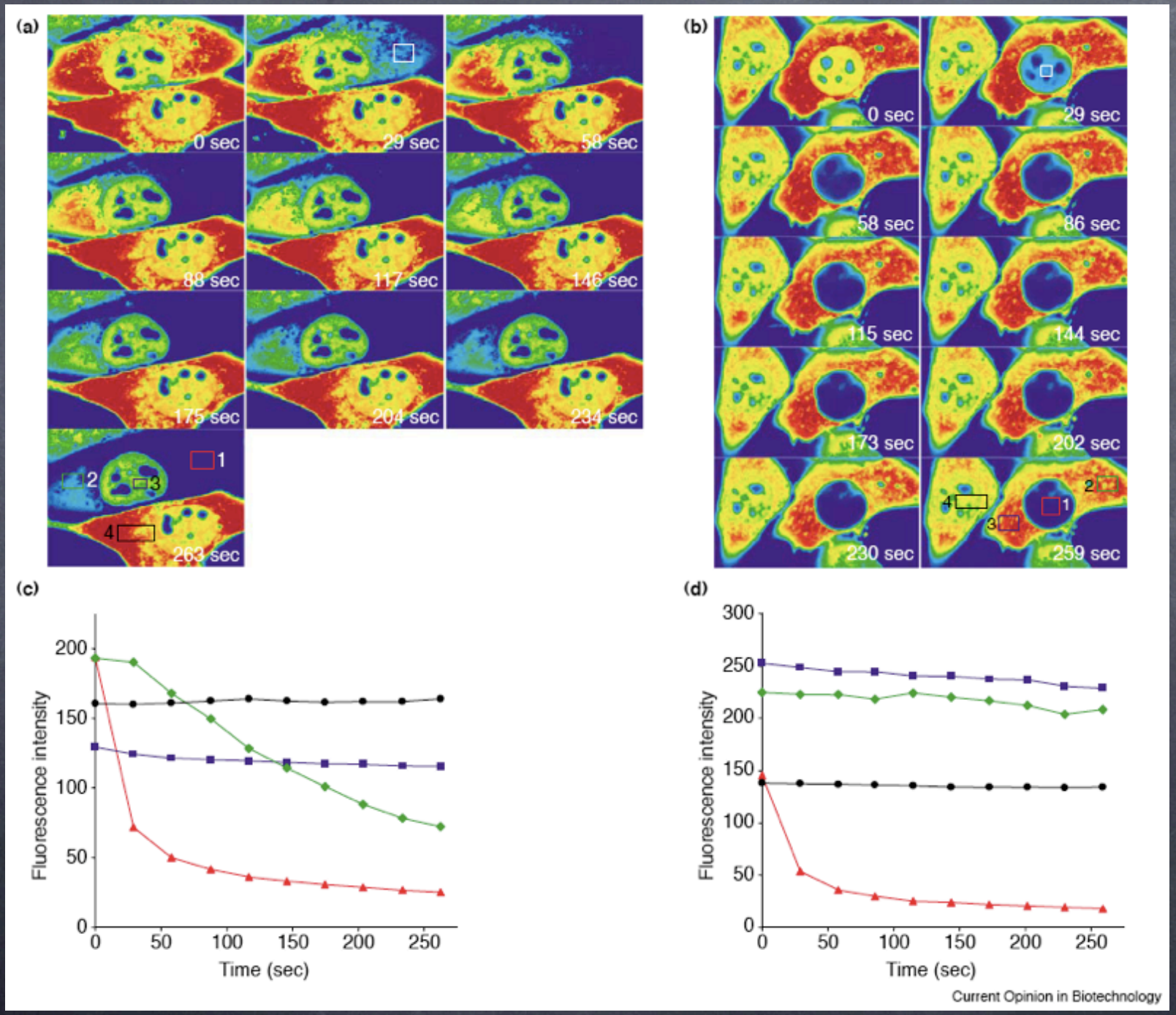

Total Internal Reflectance Fluorescence (TIRF) Microscopy:

sub plasma membrane events

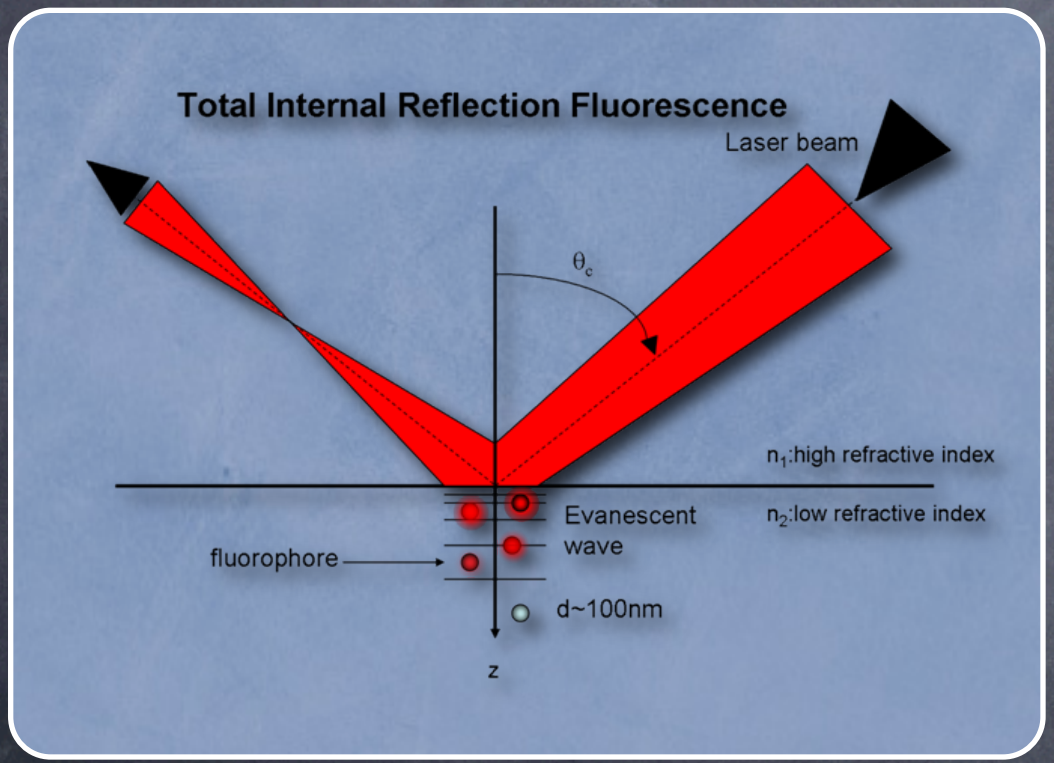

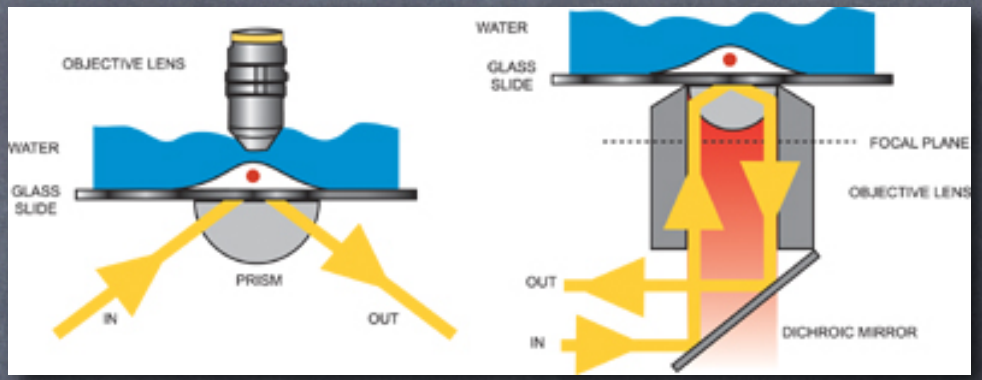

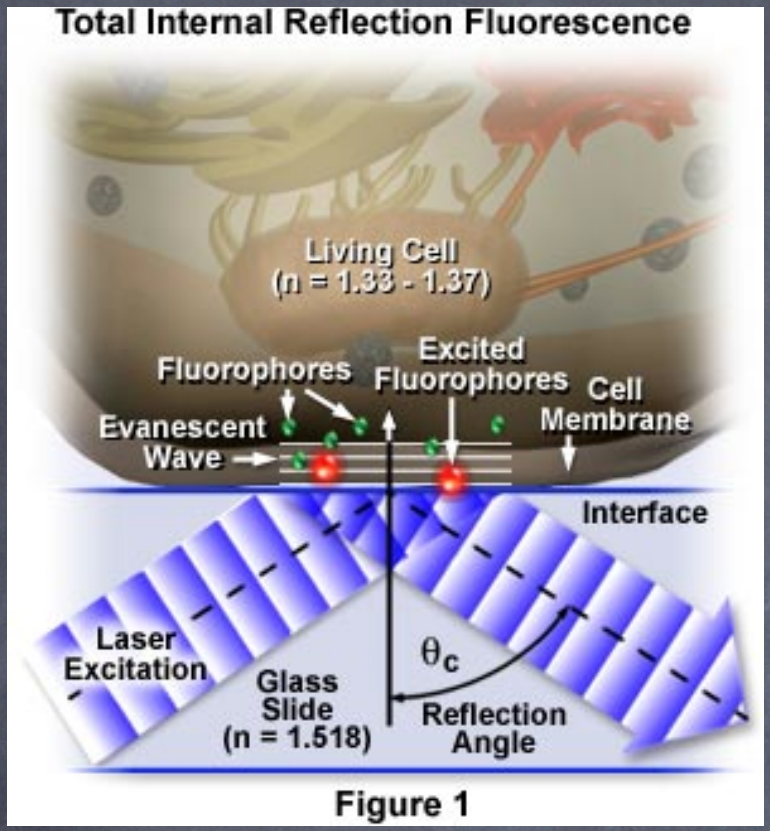

Figure 1

Snell law

$$n_1 \sin\theta_1 = n_2 \sin\theta_2$$

$$\theta_{crit} = \arcsin\left(\frac{n_2}{n_1}\right) = \text{critical angle}$$

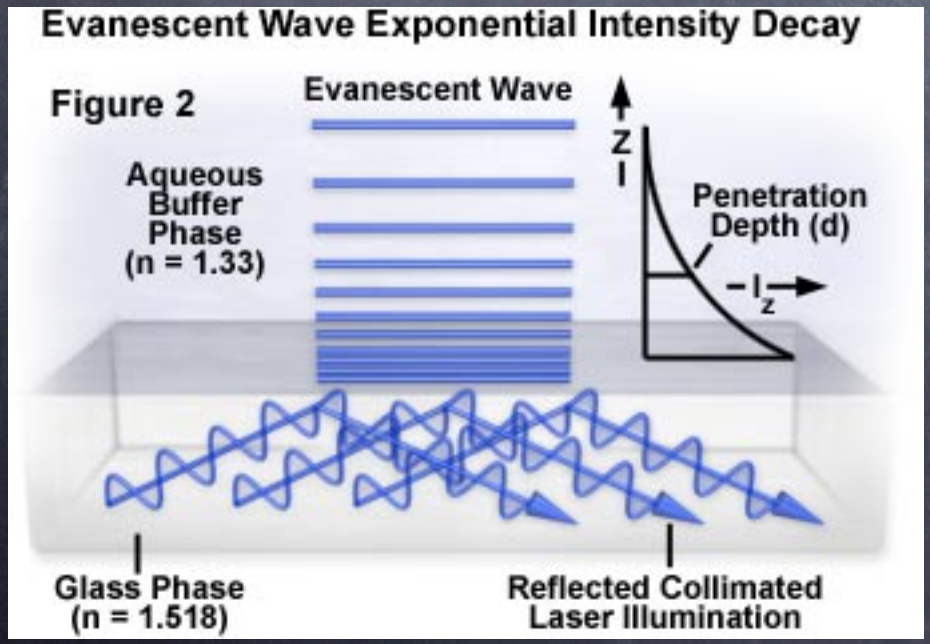

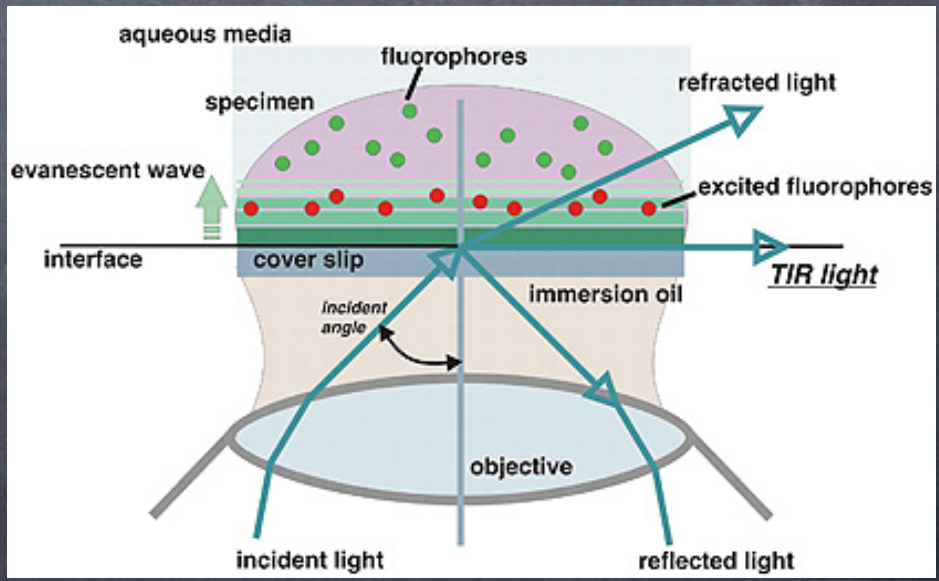

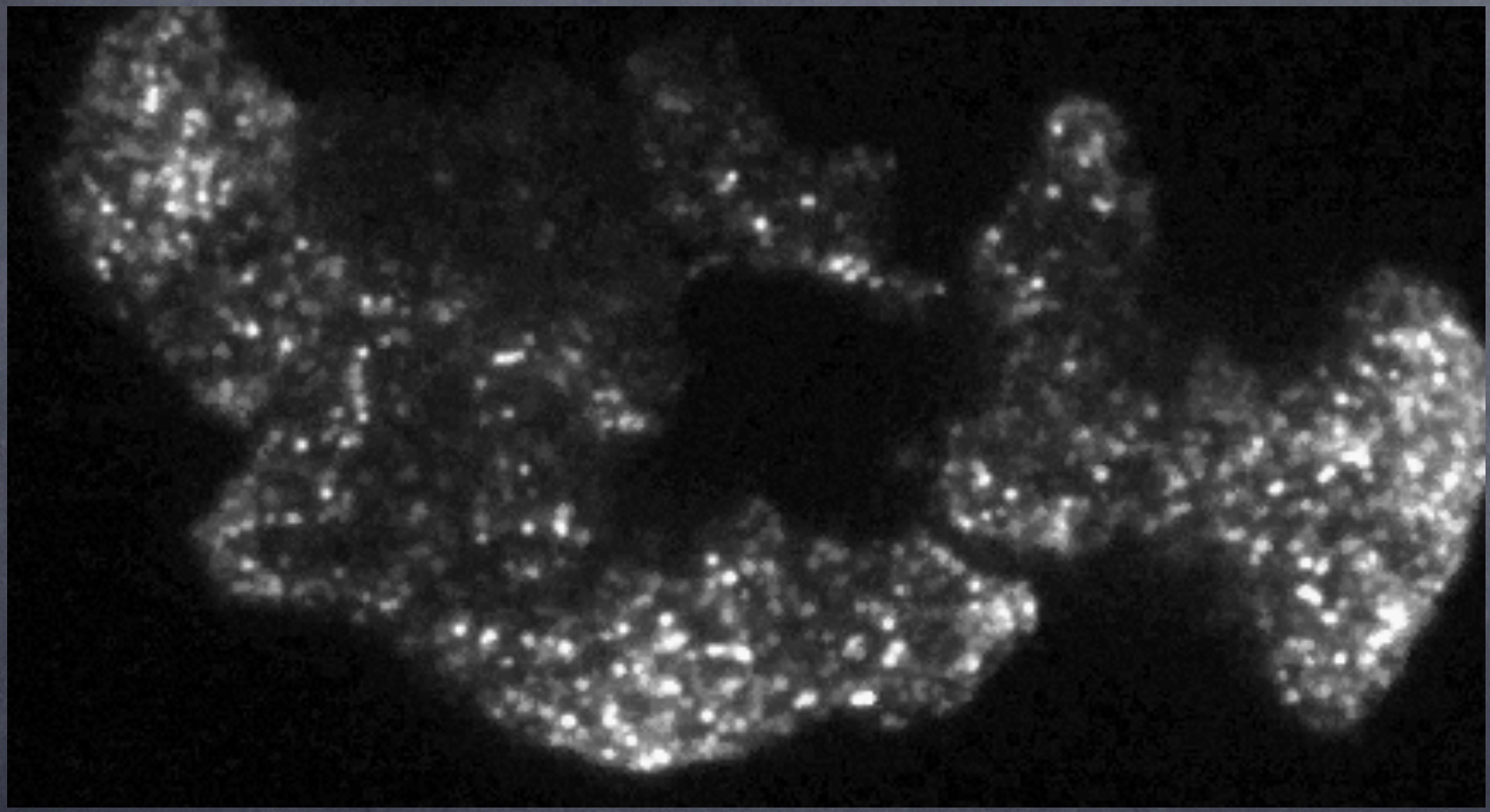

REVIEW

nature chemical biology

Imaging single events at the cell membrane

Jyoti K Jaiswal & Sanford M Simon

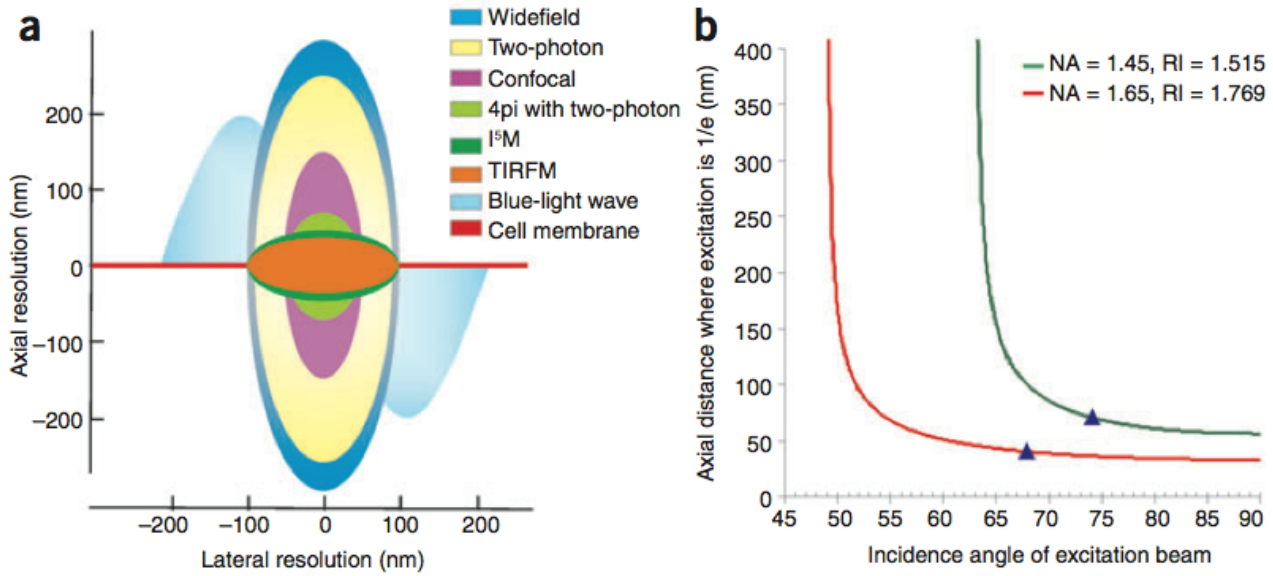

Figure 1 Resolution of various optical imaging approaches. (**a**) Estimated axial and lateral resolutions of various optical imaging approaches. The size of a single wave of blue light and axial thickness of cell membrane are drawn for the sake of comparison. The figure is partly redrawn with permission from ref. 61. (**b**) Distance over which the evanescent field decays to 1/e is a function of the refractive index of the glass and the angle of incidence of the excitation light. This has been drawn for two objectives, each with a different numerical aperture (NA) and refractive index (RI). The maximum angle that can be obtained by "through the objective" excitation is indicated by arrowheads for each objective.

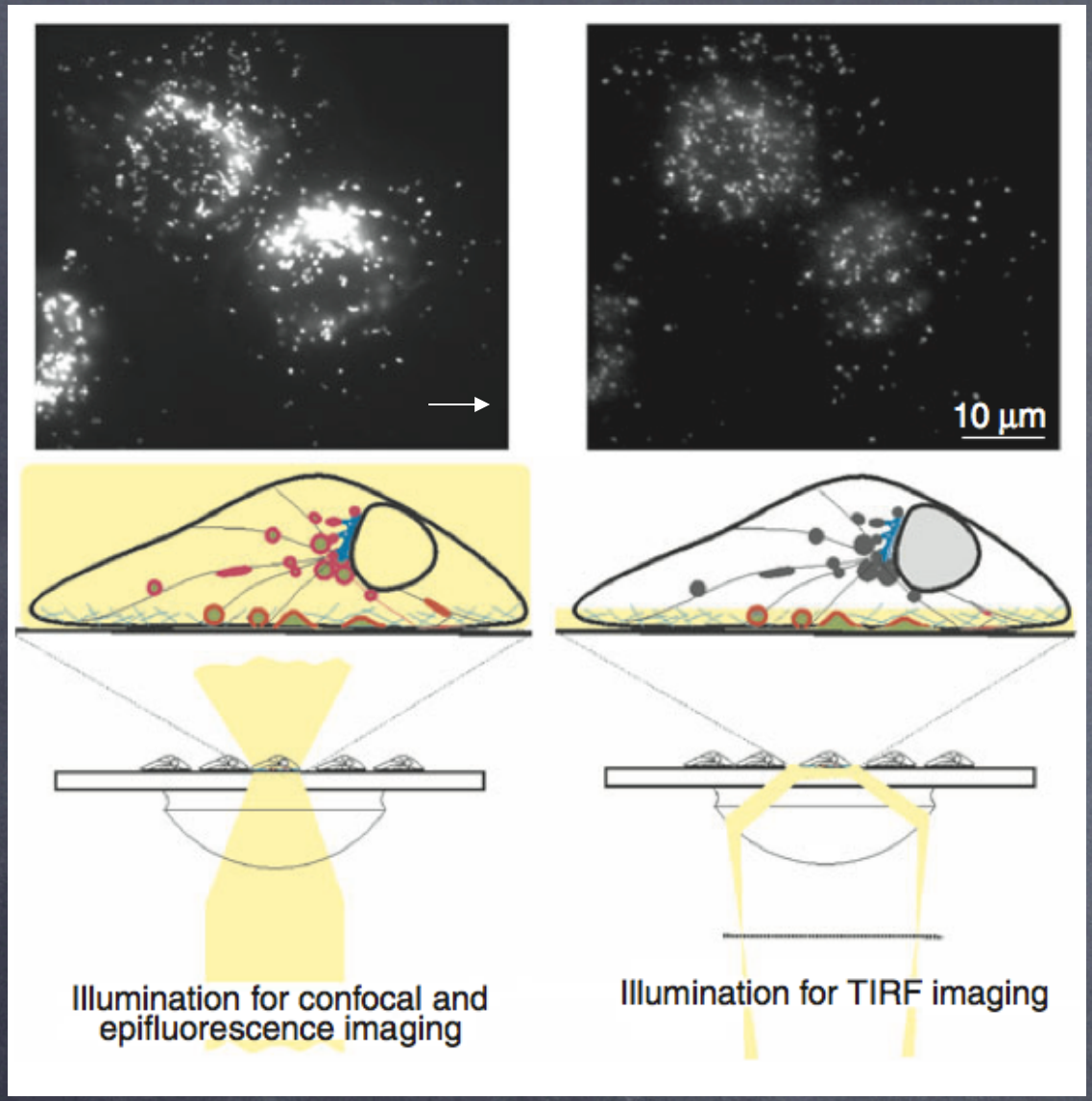

Figure 2 Comparison of wide-field and TIRF imaging. Lysosomes labeled with fluorescent dextran were imaged in the same focal plane by wide-field epifluorescence microscopy (top left) and TIRFM (top right). Images adapted with permission from *The Journal of Cell Biology*, 2002, **159**, 625-635. Copyright 2002 The Rockefeller University Press. In epifluorescence or confocal microscopy, laser light excites fluorophores throughout the cell (bottom left). In contrast, in TIRFM, the illumination decreases exponentially from the cover slip to 1/e within a distance roughly one quarter to one tenth of the wavelength of light (bottom right).

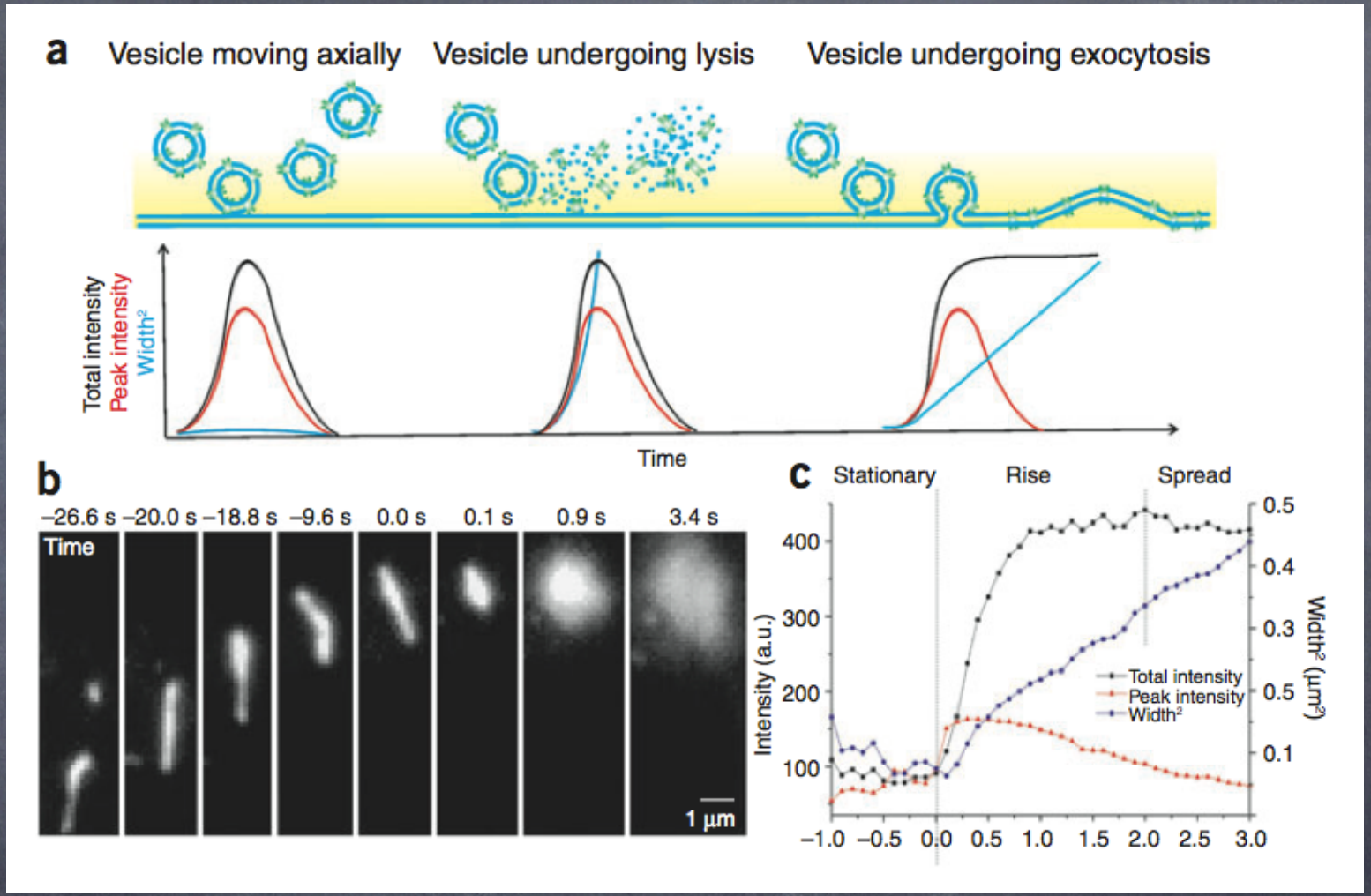

Figure 3 Use of TIRFM to study behavior of individual vesicles near the cell membrane. (**a**) Top panel shows three behaviors of vesicles near the cell surface as they enter the evanescent field (shaded yellow region). The vesicle in the left panel moves axially, entering the evanescent field and then retreating. The vesicle in the middle lyses upon entering the evanescent field. The vesicle on the right fuses to the membrane. Lower panel shows the predicted changes in peak intensity, total intensity and width of the fluorescence of the fluorescent cargo (green cylinders) in the membrane of the vesicle. (**b**) A single vesicle labeled with a GFP-tagged membrane protein (vesicular stomatitis virus glycoprotein) is observed to approach, move along the membrane, pause, and then undergo a lateral spread of its fluorescence[63]. (**c**) Quantification of fluorescence from the vesicle in **b**[63]. a.u., arbitrary units.

Am J Physiol Gastrointest Liver Physiol 291: G146–G155, 2006.
First published February 16, 2006; doi:10.1152/ajpgi.00003.2006.

Measurement of Ca^{2+} signaling dynamics in exocrine cells with total internal reflection microscopy

Jong Hak Won and David I. Yule

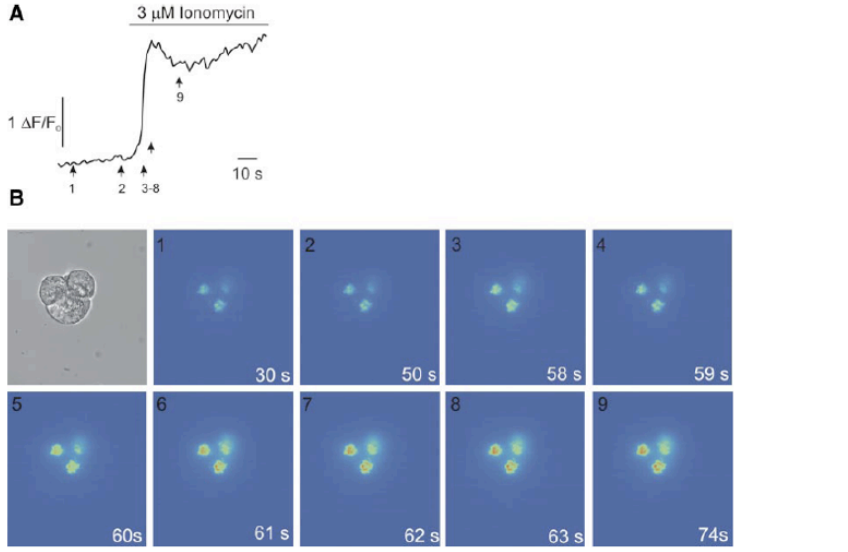

Fig. 2. Ca^{2+} measurement using TIRFM. Under conditions established in Fig. 1, intracellular Ca^{2+} {$[Ca^{2+}]_i$} was measured using TIRFM. *A*: line profile of average fluorescence in a polygon corresponding to the original region subject to TIRFM. *B*: series of images obtained from a small pancreatic acinus at the time points indicated in *A*. ΔF/F0, changes in Fluo-4 fluorescence.

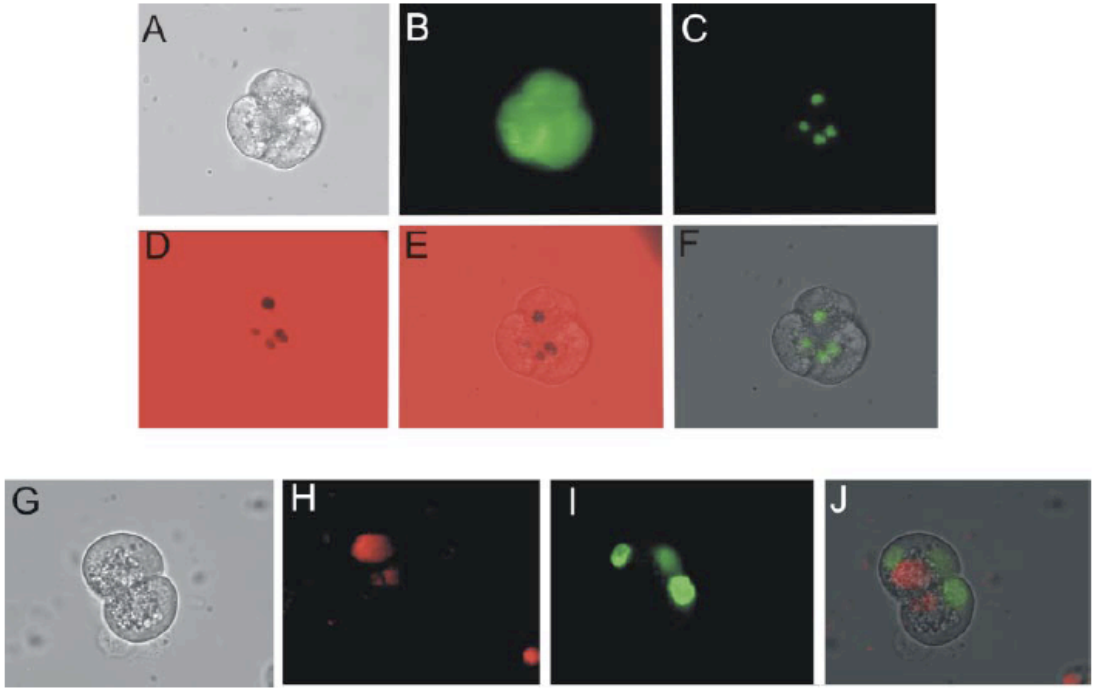

Fig. 1. Establishing total internal reflection fluorescence microscopy (TIRFM) excitation in exocrine cells. *A*: bright-field image of a small pancreatic acinus, prepared as described in MATERIALS AND METHODS. In *B*, the acinus depicted in *A* was loaded with fluo-4 (4 μM), and the dye was excited using the 488-nm argon-krypton laser line in wide-field mode (WFM). In *C*, the dye was excited following total internal reflection of the incident excitation light. In *D*, rhodamine-dextran (100 μM) in the external solution was excited using TIRFM with the 568-nm laser line. *E*: overlay images of *A*, *C*, and *D*. *F*: overlay image of *A* and *C*. *G*: bright-field image of a doublet of pancreatic acinar cells. *H*: TIRFM of cells shown in *G* following rhod-2 loading. *I*: staining of nuclei with SYTO 16 (1 μM) in WFM. *J*: overlay image of *G*, *H*, and *I*.

Flash photolysis of caged compounds

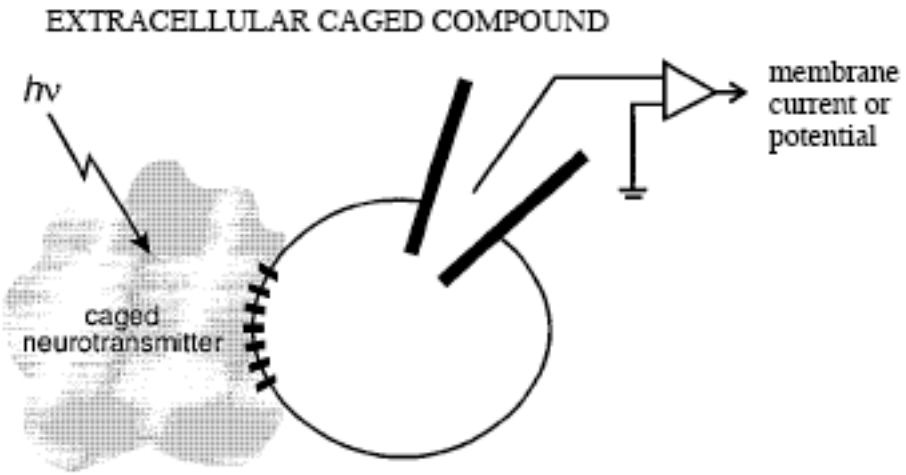

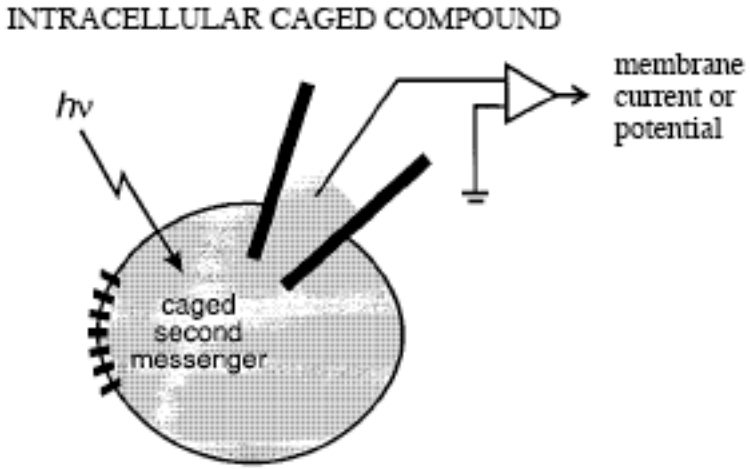

photon energy

$E = h\nu$

h = Planck constant

ν = frequency

absorbance of a caged compound $A = \varepsilon c l$

$M + h\nu \rightarrow M^*$ < 1 ns

$M^* \rightarrow products$ dark reactions (μs - ms)

$$\varphi = \frac{\text{product}}{\text{absorbed photons}} = \text{quantum yield}$$

Table 1. *Properties and sources of commercially available caged compounds*

Caged compound	Source	Structure	ε ($M^{-1}cm^{-1}\times10^{-3}$)	ϕ	release half time (ms)	*Useful concentration range
Intracellular probes						
ATP	C, M	NPE	17.5 at 260 nm	0.63	7	5-20 mM
	M	DMNPE	5.3 at 354 nm			
ADP	M	NPE	19.6 at 260 nm		8.7	1-20 mM
GTP	C	NPE	~16.9 at 255 nm			1-10 mM
GTP-γ-S	M	NB				1-10 mM
	M	DMNB	4.8 at 355 nm			
	M	NPE	15.4 at 260 nm	0.35	6	
	M	DMNPE	3.6 at 362 nm			
GDP-β-S	M	DMNPE	~16.9 at 260 nm			1-10 mM
cyclic AMP	C, M	NPE	20 at 259 nm			50-500 μM
	M	DMNB	4 at 350 nm		<5	
cyclic GMP	C, M	NPE				50-500 μM
Inositol 1,4,5-trisphosphate	C	NPE	4.2 at 200 nm	0.65	3	1-500 μM
Inorganic phosphate	M	NPE	4.2 at 260 nm	0.54	<0.1	up to 20 mM
Calcium:						
nitr-5	C	see text	see Table 2			0.2 - 10 mM
nitr-7	C					
DM-nitrophen	C					
calcium chelator:						
diazo-2	M					
Extracellular probes						
carbachol	C, M	NPE	5.2 at 262 nm	0.29	0.07	50 -100 μM
	M	CNB	5.2 at 266 nm	0.8	0.04	
adrenaline	M	DMNB				50-500 μM
noradrenaline	M	DMNBOC				50-500 μM
dopamine	M	DMNBOC				50-500 μM
isoprenaline	M	NB				50-500 μM
propranolol	M	NB				100 -500 μM
serotonin	M	DMNBOC				50-500 μM
glutamate	M	DMNB	5.7 at 347 nm			up to 20 mM
MK-801	M	DMNBOC				100-500 μM
aspartate	M	DMNB	6.0 at 347 nm			50-500 μM
GABA	M	DMNB	5.4 at 347 nm			50-500 μM
glycine	M	DMNB	5.7 at 345 nm			50-500 μM
arachidonic acid	M	DMNB				
nitric oxide	M,A, 1	$K_2Ru(NO)Cl_5$	0.56 at 320 nm	0.06	<5	0.5-50 μM

NP-EGTA

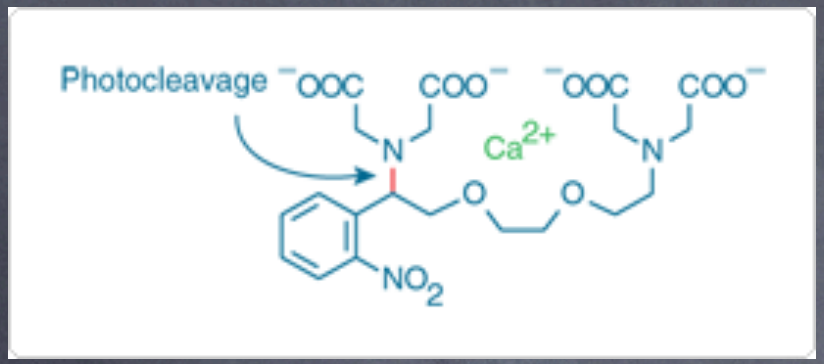

DMNP-EDTA

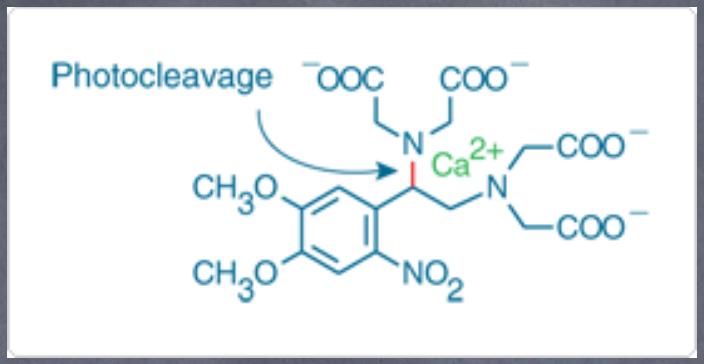

1) Voltage

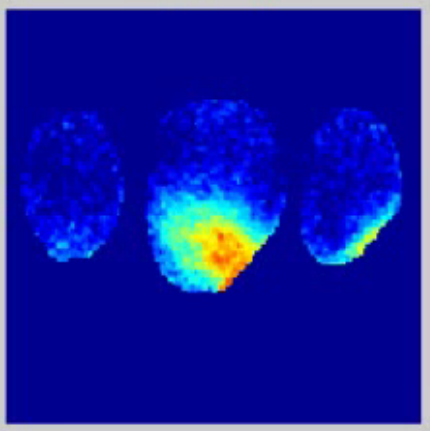

NP-EGTA caged Ca2+voltage probe

2) Calcium

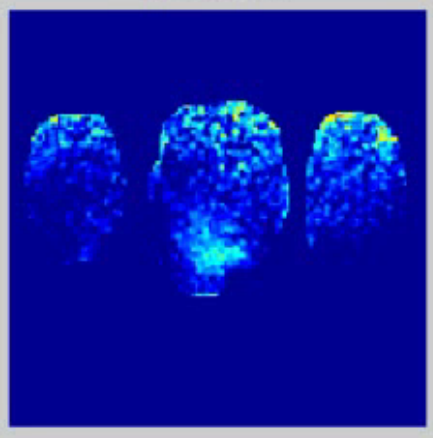

NP-EGTA caged Ca2+X-Rhod calcium probe

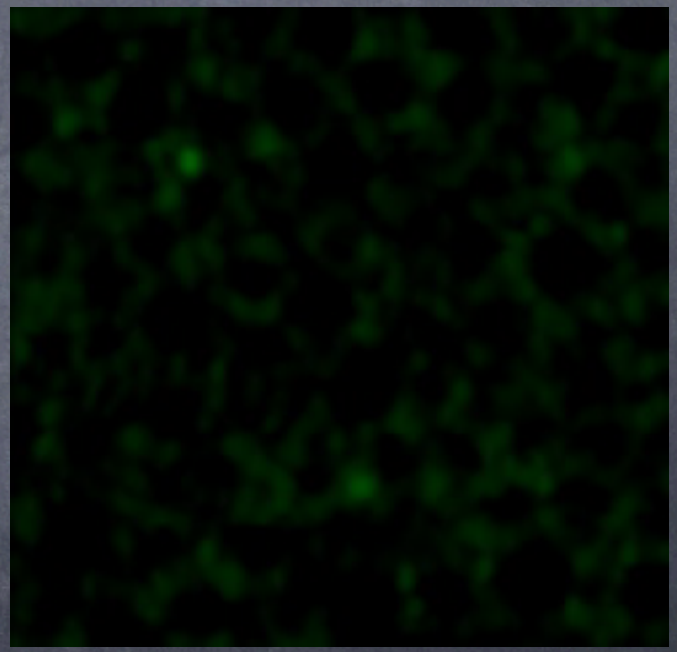

NPE caged InsP3+ Texas Red granules (Xenopus eggs)

jove Journal of Visualized Experiments www.jove.com

Video Article

Flash Photolysis of Caged Compounds in the Cilia of Olfactory Sensory Neurons

Anna Boccaccio[1,2], Claudia Sagheddu[1], Anna Menini[1,3]

[1]SISSA, International School for Advanced Studies
[2]Istituto di Biofisica, Consiglio Nazionale delle Ricerche
[3]SISSA Unit, Italian Institute of Technology

Photolysis of caged compounds allows the production of rapid and localized increases in the concentration of various physiologically active compounds[1]. Caged compounds are molecules made physiologically inactive by a chemical cage that can be broken by a flash of ultraviolet light. Here, we show how to obtain patch-clamp recordings combined with photolysis of caged compounds for the study of olfactory transduction in dissociated mouse olfactory sensory neurons. The process of olfactory transduction (Figure 1) takes place in the cilia of olfactory sensory neurons, where odorant binding to receptors leads to the increase of cAMP that opens cyclic nucleotide-gated (CNG) channels[2]. Ca entry through CNG channels activates Ca-activated Cl channels. We show how to dissociate neurons from the mouse olfactory epithelium[3] and how to activate CNG channels or Ca-activated Cl channels by photolysis of caged cAMP[4] or caged Ca[5]. We use a flash lamp[6,7] to apply ultraviolet flashes to the ciliary region to uncage cAMP or Ca while patch-clamp recordings are taken to measure the current in the whole-cell voltage-clamp configuration [8-11].

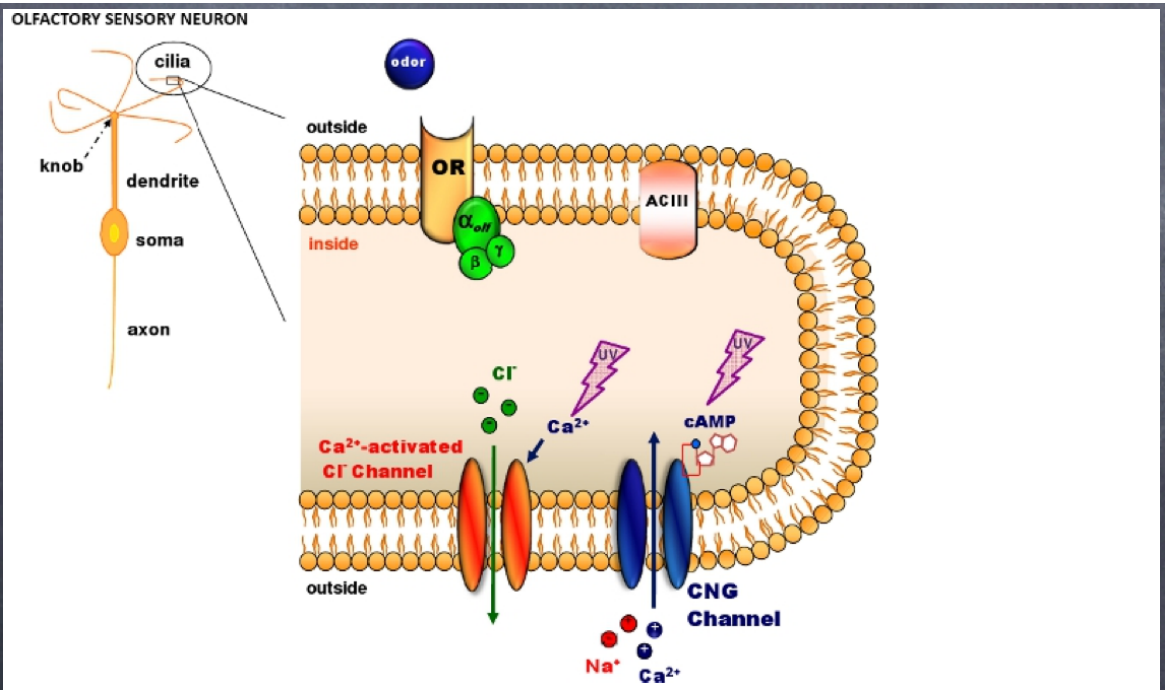

Figure 1. Olfactory transduction in the cilia of olfactory sensory neurons. Odorant molecules bind to odorant receptors (OR) activating a G protein that in turns activates adenylyl cyclase (ACIII) producing an intracellular increase in cAMP. cAMP opens cyclic nucleotide-gated (CNG) channels allowing the entry of Na and Ca ions. The intracellular Ca increase activates Ca-activated Cl channels. Caged cAMP or caged Ca can be introduced in the cilia diffusing through a patch pipette. A flash of UV light produces photolysis of the caged compound (Modified, with permission, from Pifferi *et al*. 2006[2]).

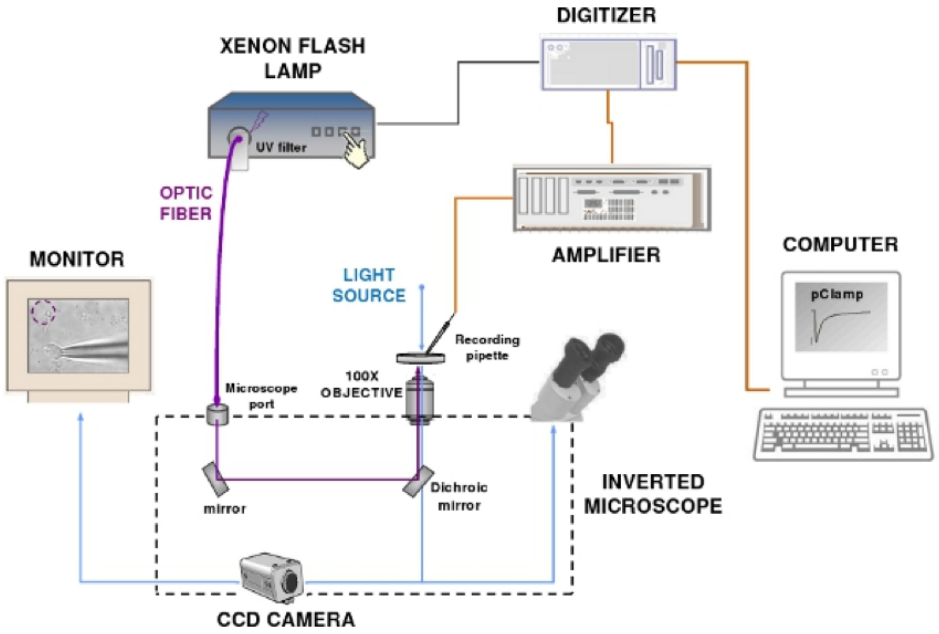

Figure 2. The patch-clamp recording and flash photolysis system. The set-up components include a patch-clamp amplifier, a computer, a digitizer, an epifluorescence microscope, a Xenon flash lamp, a CCD camera and a monitor. Blue and violet lines indicate respectively the visible and UV light path.

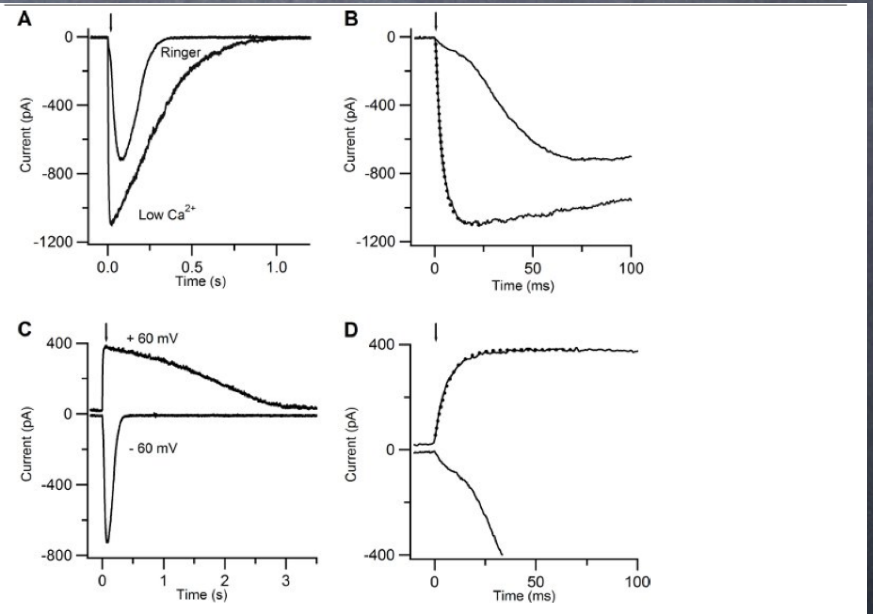

Figure 5. Current responses induced by photolysis of caged cAMP in low Ca and in Ringer solutions. (A) An olfactory sensory neuron was bathed in Ringer solution containing 1 mM Ca or in low Ca solution at the holding potential of -60 mV. A UV flash was released at the time indicated by the arrow. (B) Current responses plotted on an expanded timescale showed a multiphasic rising phase in Ringer, while the rising phase was well fitted with a single exponential function (dotted line) with a time constant of 3.5 ms for the response recorded in low Ca solution. (C) Currents responses from the same neuron shown in (A) bathed in Ringer's solution at the holding potential of -60 and +60 mV. (D) Current responses plotted on an expanded timescale displayed a multiphasic rising phase at -60 mV, whereas at +60 mV the rising phase was well fitted by a single exponential with a time constant of 6.7 ms (dotted line).

CONFOCAL MICROSCOPY

optical sections and 3D reconstruction

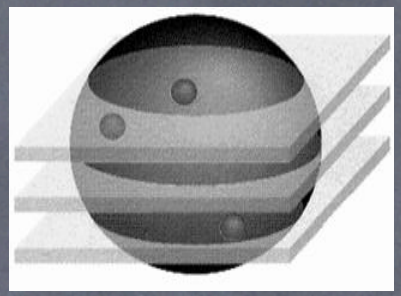

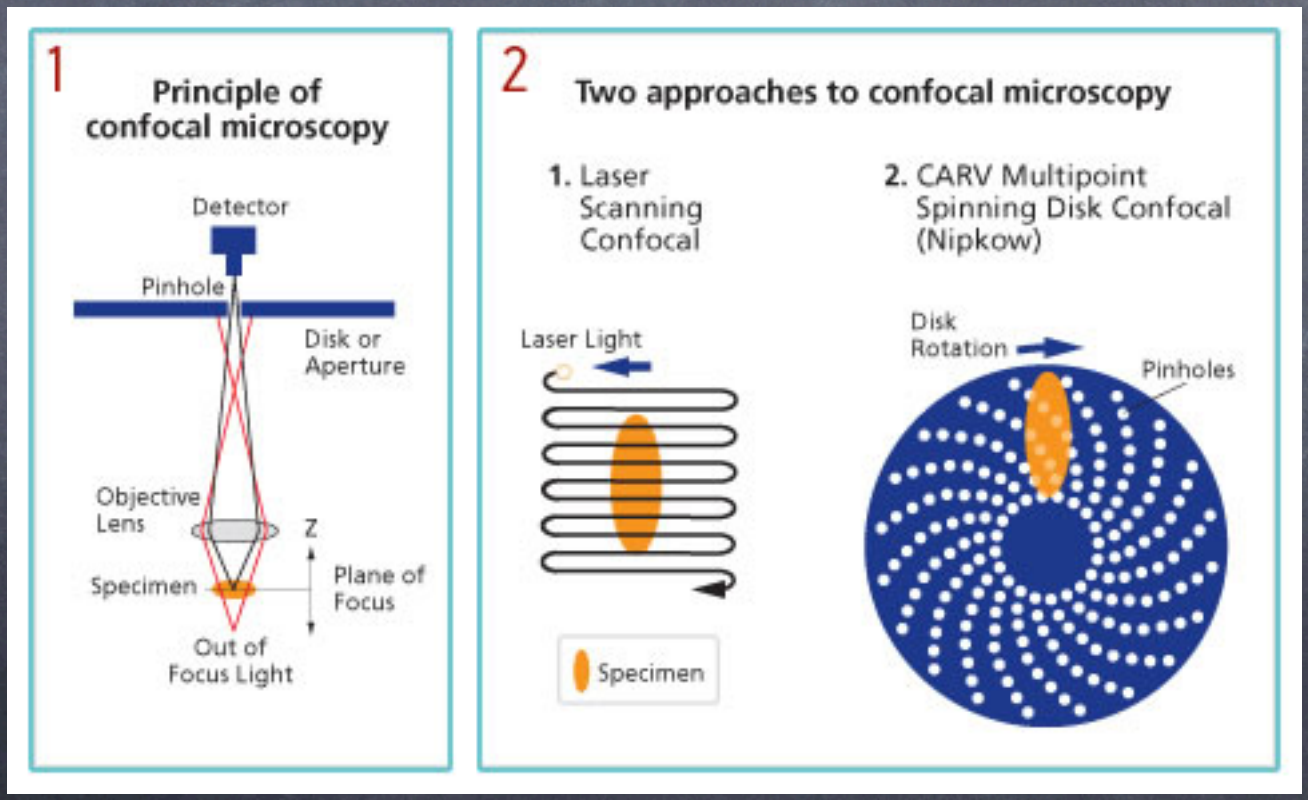

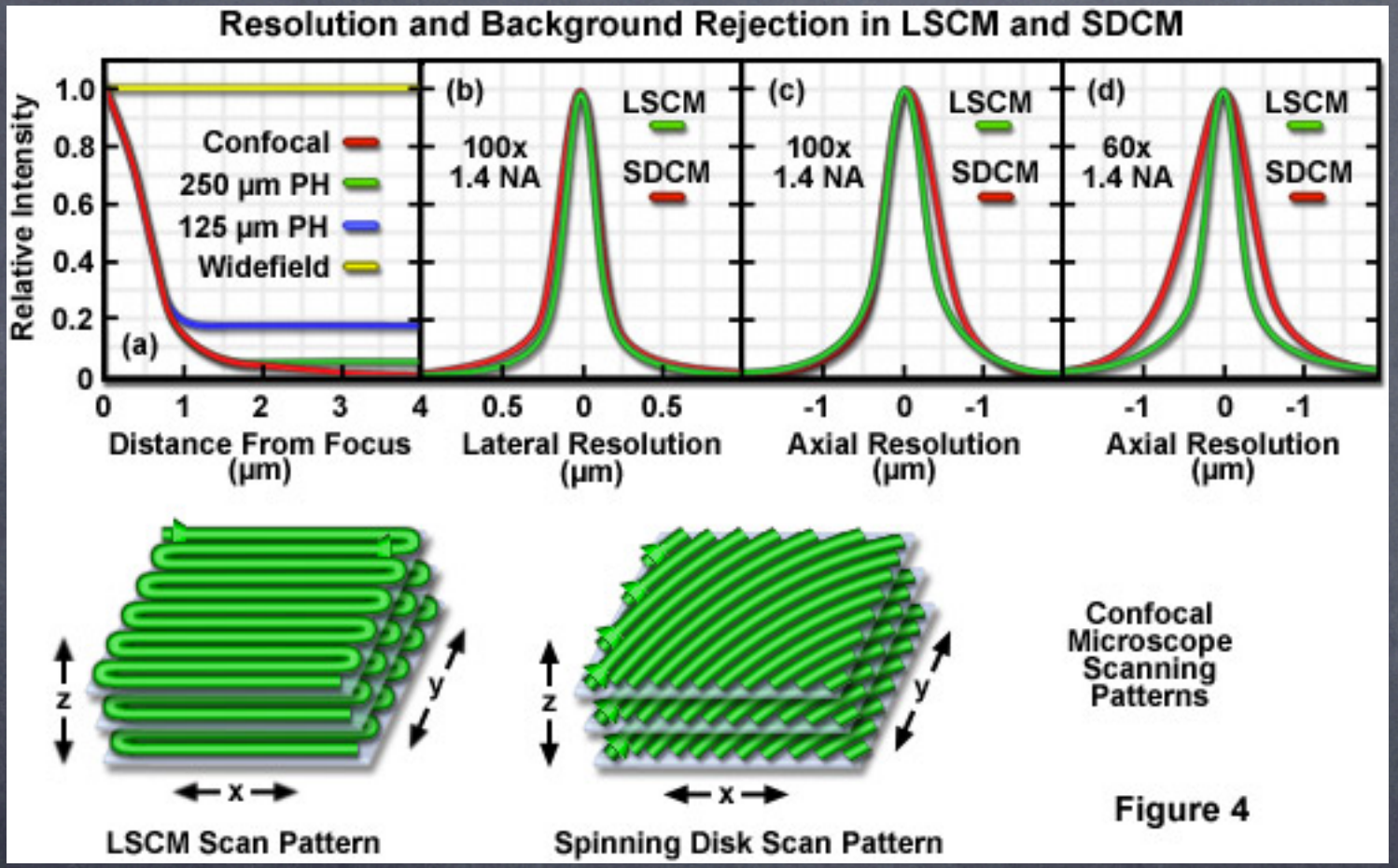
Resolution and Background Rejection in LSCM and SDCM
Relative Intensity
1.0
0.8
0.6
0.4
0.2
0
(a)
Confocal
250 µm PH
125 µm PH
Widefield
0 1 2 3 4
Distance From Focus (µm)
(b)
100x
1.4 NA
LSCM
SDCM
0.5 0 0.5
Lateral Resolution (µm)
(c)
100x
1.4 NA
LSCM
SDCM
-1 0 -1
Axial Resolution (µm)
(d)
60x
1.4 NA
LSCM
SDCM
-1 0 -1
Axial Resolution (µm)
z
y
x
LSCM Scan Pattern
z
y
x
Spinning Disk Scan Pattern
Confocal Microscope Scanning Patterns
Figure 4

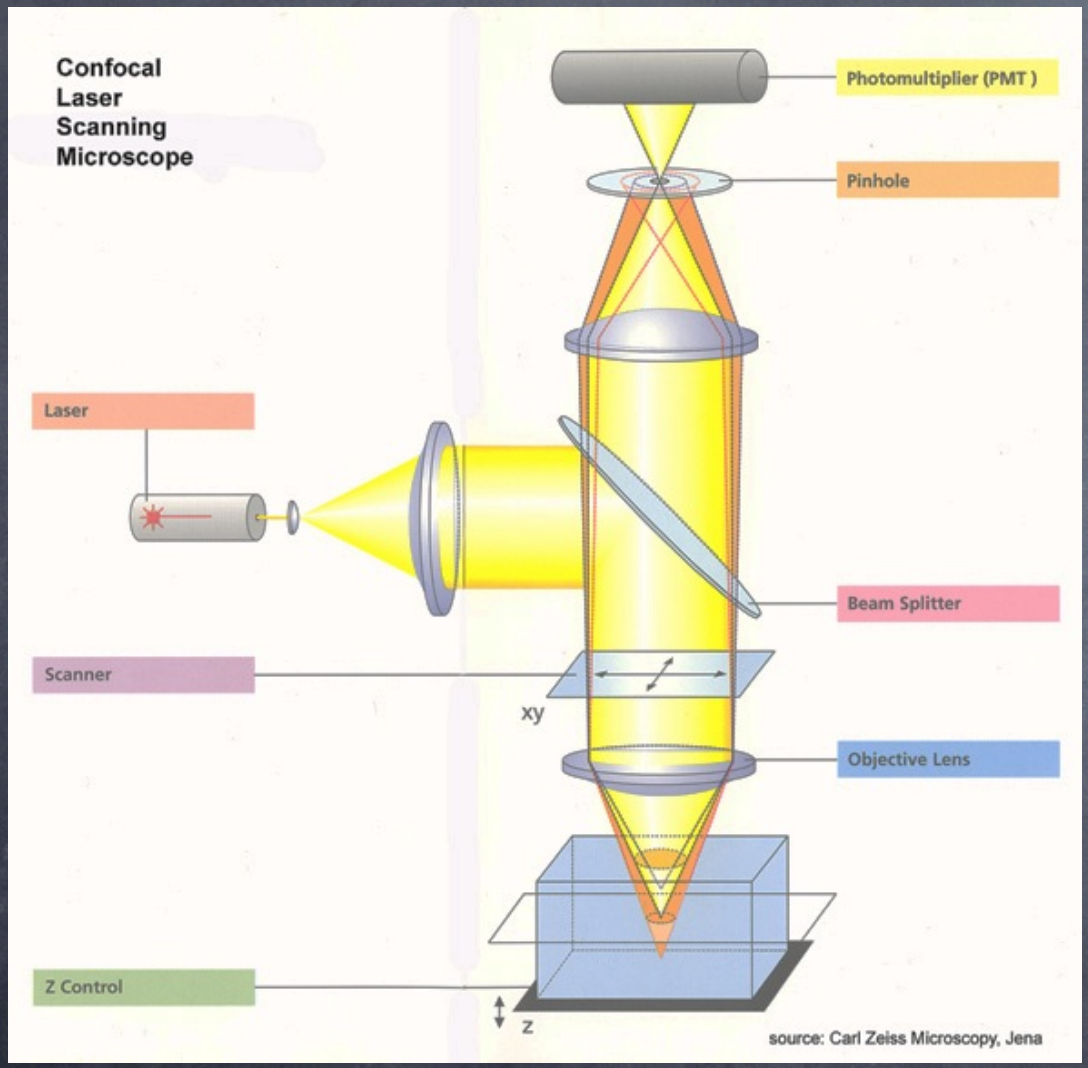
Confocal
Laser
Scanning
Microscope
Photomultiplier (PMT)
Pinhole
Laser
Beam Splitter
Scanner
xy
Objective Lens
Z Control
z
source: Carl Zeiss Microscopy, Jena

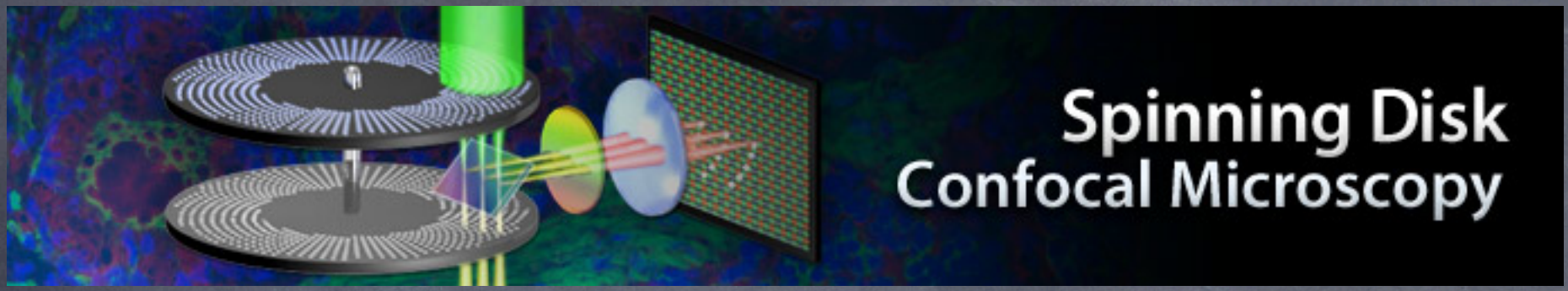
Spinning Disk
Confocal Microscopy

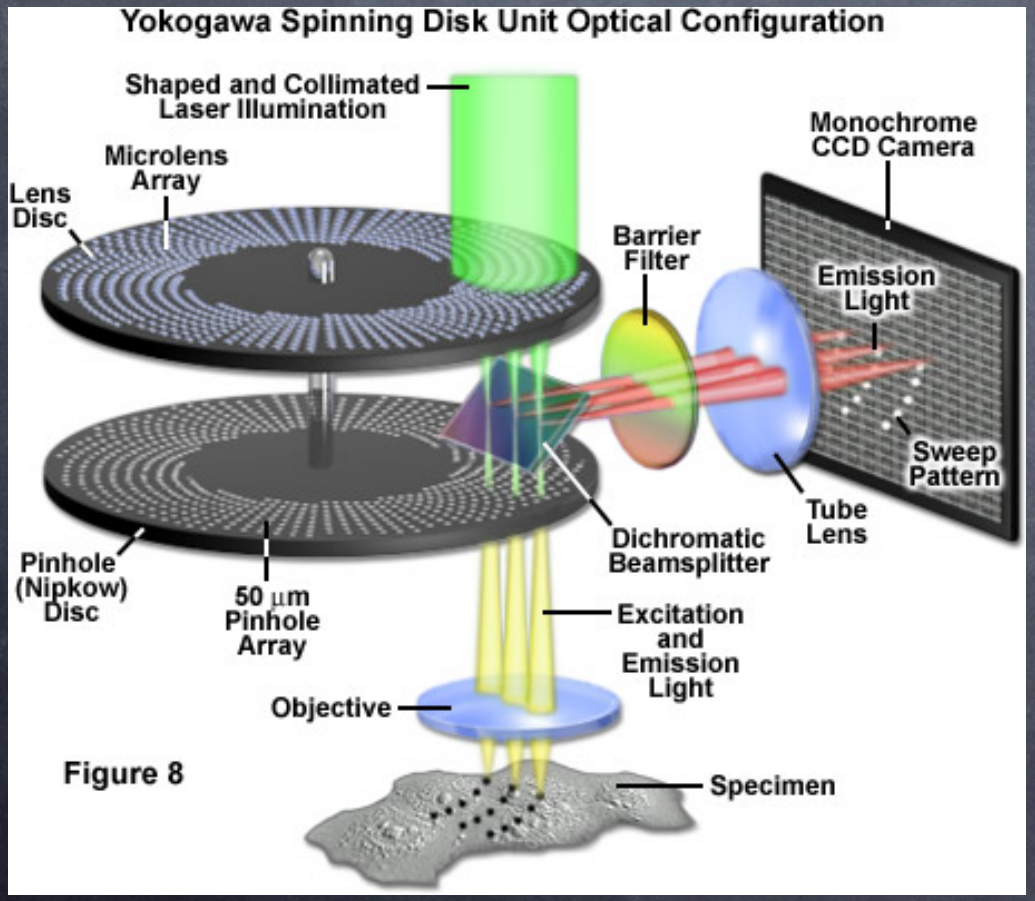
Yokogawa Spinning Disk Unit Optical Configuration
Shaped and Collimated Laser Illumination
Microlens Array
Lens Disc
Monochrome CCD Camera
Barrier Filter
Emission Light
Sweep Pattern
Tube Lens
Dichromatic Beamsplitter
Pinhole (Nipkow) Disc
50 µm Pinhole Array
Excitation and Emission Light
Objective
Specimen
Figure 8

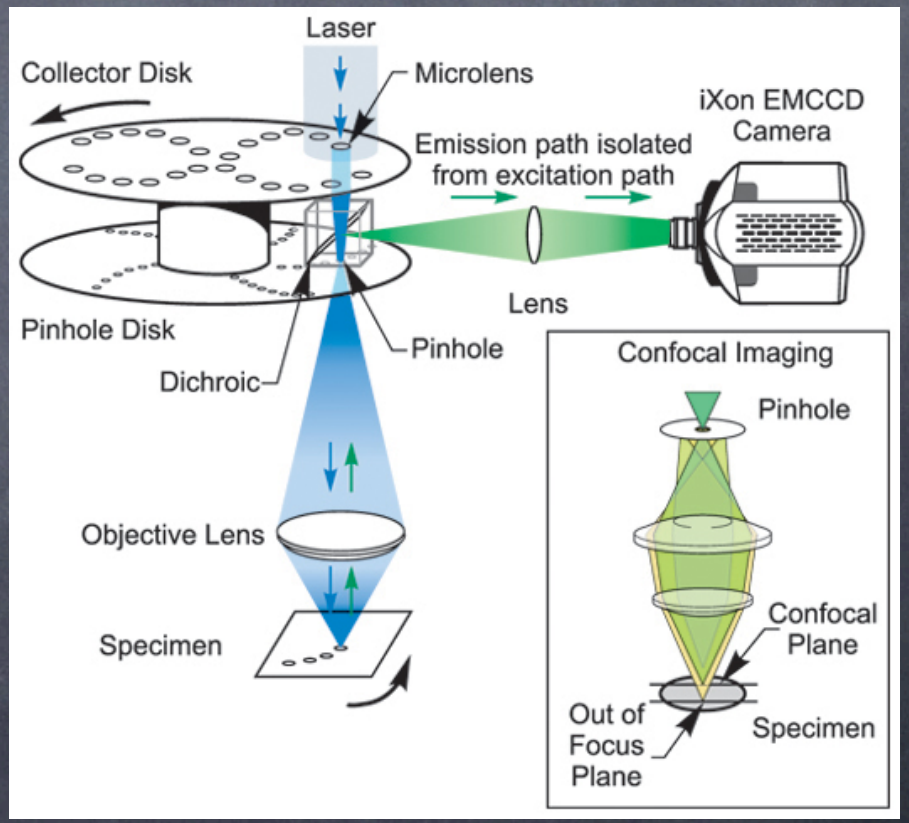
Laser
Collector Disk
Microlens
iXon EMCCD Camera
Emission path isolated from excitation path
Lens
Pinhole Disk
Pinhole
Dichroic
Objective Lens
Specimen
Confocal Imaging
Pinhole
Confocal Plane
Out of Focus Plane
Specimen

Multiphoton microscopy

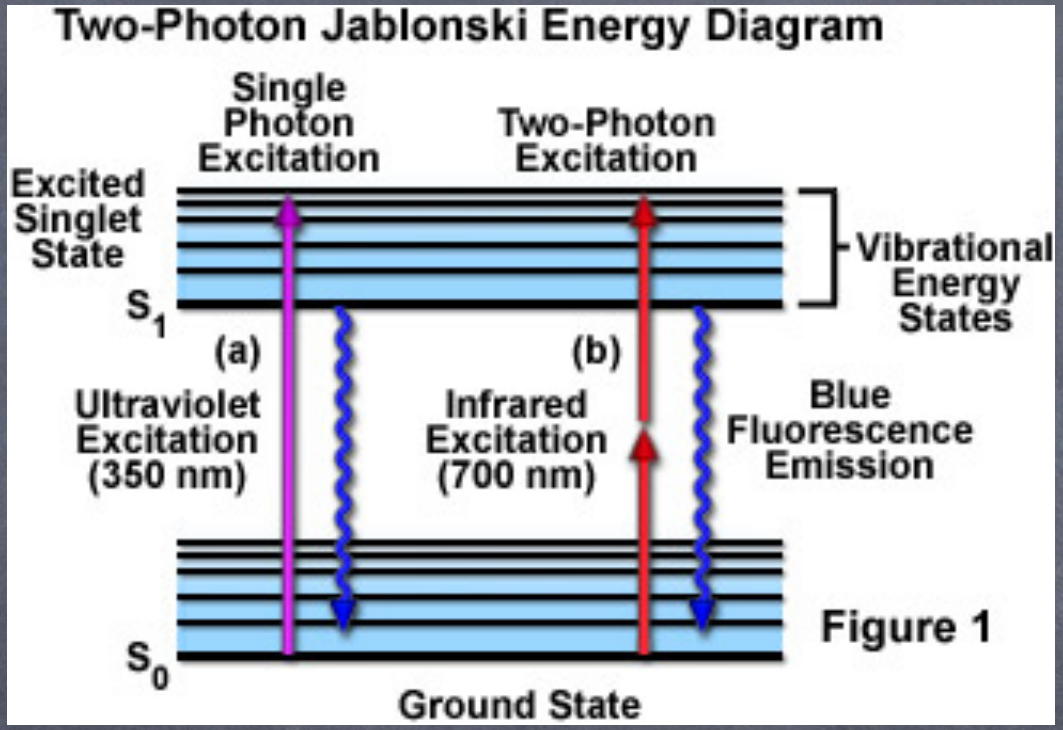

Figure 1

1-photon

2-photon